Acta Crystallographica Section D
Biological Crystallography
ISSN 0907-4449

Structure of the DNA (6–4) photoproduct dTT(6–4)TT in complex with the 64M-2 antibody Fab fragment implies increased antibody-binding affinity by the flanking nucleotides

Hideshi Yokoyama,[a]* Ryuta Mizutani,[b] Yoshinori Satow,[c] Kousuke Sato,[d] Yasuo Komatsu,[e] Eiko Ohtsuka[e] and Osamu Nikaido[f]

[a]School of Pharmaceutical Sciences, University of Shizuoka, Japan, [b]Department of Applied Biochemistry, School of Engineering, Tokai University, Japan, [c]Graduate School of Pharmaceutical Sciences, University of Tokyo, Japan, [d]Faculty of Pharmaceutical Sciences, Hokkaido University, Japan, [e]Bioproduction Research Institute, National Institute of Advanced Industrial Science and Technology (AIST), Japan, and [f]Department of Food and Nutrition, Kanazawa Gakuin College, Japan

Correspondence e-mail: h-yokoya@u-shizuoka-ken.ac.jp

Received 21 October 2011
Accepted 4 January 2012

PDB Reference: dTT(6–4)TT–64M-2 Fab fragment complex, 1keg.

Pyrimidine (6–4) pyrimidone DNA photoproducts produced by ultraviolet light are highly mutagenic and carcinogenic. The crystal structure of the dTT(6–4)TT photoproduct in complex with the Fab fragment of the antibody 64M-2 that is specific for (6–4) photoproducts was determined at 2.4 Å resolution. The dT(6–4)T segment is fully accommodated in the concave binding pocket of the Fab, as observed in the complex of dT(6–4)T with the Fab. The pyrimidine and pyrimidone bases of the dT(6–4)T segment are positioned nearly perpendicularly to each other. The thymidine segments flanking both ends extend away from the dT(6–4)T segment. The 5′-side thymine base is parallel to the side chain of Tyr100iH of the antibody heavy chain and is also involved in electrostatic interactions with Asn30L, Tyr32L and Lys50L of the antibody light chain. The 5′-side and 3′-side phosphate groups exhibit electrostatic interactions with Asn28L and Ser58H, respectively. These interactions with the flanking nucleotides explain why longer oligonucleotides containing dT(6–4)T segments in the centre show higher antibody-binding affinities than the dT(6–4)T ligand.

1. Introduction

DNA photoproducts produced by ultraviolet irradiation cause mutations, cellular transformation and cell death (Setlow, 1978). Pyrimidine (6–4) pyrimidone DNA photoproducts (Fig. 1) are as predominant as cyclobutane pyrimidine dimers, but are more mutagenic (LeClerc *et al.*, 1991).

A crystal structure containing the dT(6–4)T segment has been determined as a complex with an antibody Fab fragment (Yokoyama *et al.*, 2000). The structure indicated that the dT(6–4)T molecule was in a closed circular form and that the 6–4-linked thymine bases were perpendicular to each other.

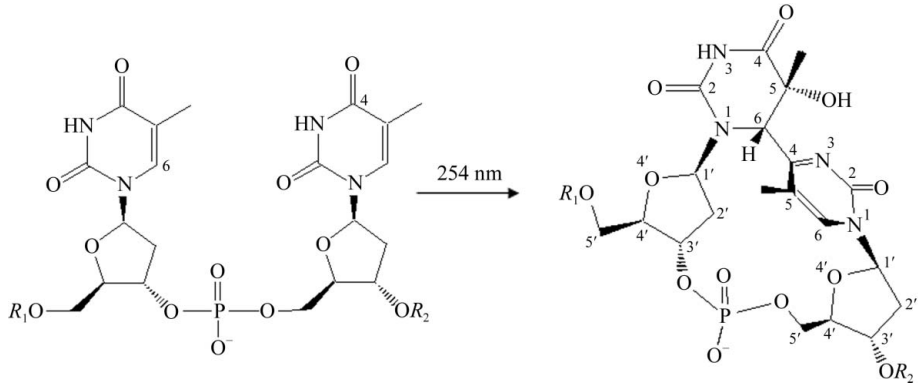

Figure 1
A DNA (6–4) photoproduct formed by ultraviolet irradiation. (*a*) Normal DNA; (*b*) dT(6–4)T photoproduct. The atom numbering used is shown for the central dT(6–4)T segment.

These features were also observed in the NMR structures of dT(6–4)T photoproducts in solution (Rycyna & Alderfer, 1985). The NMR structure of the DNA duplex dT(6–4)T–dAA containing dT(6–4)T and dAA nucleotides showed that the 5′-side pyrimidine base of the dT(6–4)T segment retained Watson–Crick-type hydrogen bonds to the complementary adenine base, while the 3′-side pyrimidone base formed no hydrogen bonds to the complementary base (Kim *et al.*, 1995). The NMR structure of the DNA duplex dT(6–4)T–dGA containing an unmatched guanosine showed that the 5′-side and 3′-side (6–4) bases were hydrogen bonded to the adenine and guanine bases, respectively (Lee *et al.*, 1999). The dT(6–4)T–dGA duplex hence seems to form more stable base pairs than the dT(6–4)T–dAA duplex and provides a clue to understanding how T(6–4)T photoproducts frequently cause T-to-C mutations at their 3′-sides during replication of DNA (LeClerc *et al.*, 1991).

The toxic effects of UV-induced DNA damage are reduced *in vivo* by repairing photolesions using DNA photolyases and nucleotide-excision repair enzymes (Weber, 2005). Crystallographic studies of (6–4) photoproducts and the specific enzymes have been performed in order to elucidate the structural basis of photolesion repair. The crystal structure of the DNA (6–4) photolyase in complex with a DNA duplex containing a central (6–4) lesion (Maul *et al.*, 2008) revealed that the (6–4) lesion flips out of the DNA duplex into the active site. A flipped-out (6–4) lesion has also been reported in the crystal structure of the nucleotide-excision repair enzyme DDB1–DDB2 bound to (6–4)-lesion-containing DNA (Scrima *et al.*, 2008). These results suggest that the recognition of the (6–4) lesion is attained by a structural change in the (6–4)-lesion-containing DNA.

A series of monoclonal antibodies (64M-2, 64M-3 and 64M-5) has been established for the detection and quantification of (6–4) photoproducts (Mori *et al.*, 1991). These antibodies are highly specific, showing no affinity for other photoproducts or undamaged DNA (Kobayashi *et al.*, 1998). Site-directed mutagenesis and kinetic studies on single-chain Fv fragments of these antibodies (Morioka *et al.*, 1998; Kobayashi *et al.*, 1999) and the crystal structure of the dT(6–4)T complex with the 64M-2 Fab (Yokoyama *et al.*, 2000) have revealed that the specific recognition by the 64M-2 antibody is ascribable to the structural environment of the binding-site pocket, which is composed of His27dL, Tyr32L, Leu93L, Trp33H, Ser58H, Arg95H and Tyr100iH [light-chain and heavy-chain residues are numbered in accordance with Kabat *et al.* (1991) and are denoted by the suffixes L and H, respectively]. The results of a kinetic study of the 64M-5 Fab using single-stranded (6–4) photoproducts of various lengths indicated higher affinity for longer oligonucleotides, up to a hexamer, each containing the dT(6–4)T segment in the middle (Kobayashi *et al.*, 1998). An NMR study (Torizawa *et al.*, 1998) indicated that four phosphate groups on both sides of the dT(6–4)T segment are involved in interaction with the 64M-5 Fab.

In order to elucidate the structure of the (6–4) photoproduct with flanking nucleotides on both sides as well as its recognition by the antibody, the crystal structure of dTT(6–4)TT was determined as a complex with the Fab of the 64M-2 antibody, which is highly homologous to the 64M-5 antibody. The increased affinity of dTT(6–4)TT for the antibody is discussed, comparing the liganded structure with that of the dT(6–4)T complex. The use of longer oligonucleotides containing the dT(6–4)T segment allows us to elucidate the interaction of the flanking nucleotides with the antibody.

Table 1
Crystallographic data, diffraction data collection and refinement statistics.

Values in parentheses are for the highest resolution shell.

Space group	$P2_12_12_1$
Unit-cell parameters (Å)	a = 73.6, b = 137.3, c = 49.6
Resolution range	10.0–2.4 (2.49–2.40)
No. of crystals used	1
No. of observed reflections	89848 (6273)
No. of unique reflections	17570 (1502)
$R_{\rm merge}(I)$†	0.077 (0.304)
Completeness (%)	0.920 (0.802)
Average $I/\sigma(I)$	21.8 (3.0)
R‡	0.207 (0.276)
$R_{\rm free}$§	0.268 (0.392)
No. of non-H atoms	
Protein	3263
Ligand	77
Water	70
Ni^{2+}	1
Average B factors (Å^2)	
Protein	21.1
Ligand	35.2
Water	26.9
Ni^{2+}	30.6
Main-chain torsion-angle statistics (%)	
Most favoured regions	87.6
Additionally allowed regions	11.3
Generously allowed regions	0.3
Disallowed regions	0.8
R.m.s. deviations from ideality	
Bond lengths (Å)	0.008
Bond angles (°)	1.440

† $R_{\rm merge}(I) = \sum_{hkl}\sum_i |I_i(hkl) - \langle I(hkl)\rangle| / \sum_{hkl}\sum_i I_i(hkl)$. ‡ $R = \sum_{hkl} \big||F_{\rm obs}| - |F_{\rm calc}|\big| / \sum_{hkl} |F_{\rm obs}|$, where $F_{\rm obs}$ and $F_{\rm calc}$ are observed and calculated structure-factor amplitudes, respectively. § $R_{\rm free}$ is calculated for a 10% subset of all of the reflections which was not used in the crystallographic refinement.

2. Materials and methods

2.1. Crystallization of the 64M-2 Fab in complex with dTT(6–4)TT

The 64M-2 Fab was prepared as described previously (Yokoyama *et al.*, 2000). The dTT(6–4)TT ligand was synthesized as described elsewhere (Iwai *et al.*, 1996) and isolated by reversed-phase chromatography (Kobayashi *et al.*, 1998). Crystals were prepared by mixing equal volumes of a protein solution consisting of 0.2 m*M* purified 64M-2 Fab and 0.25 m*M* dTT(6–4)TT and a reservoir solution consisting of 12–16% PEG 8000, 0.1 *M* Tris–HCl pH 8.5, 10 m*M* $NiCl_2$ and were grown in a darkroom at 293 K using the hanging-drop vapour-diffusion method. Plate-shaped crystals appeared in a week and grew to mature dimensions of 0.70 × 0.30 × 0.15 mm. Crystallographic data are listed in Table 1.

2.2. Data collection and processing

Diffraction data were collected from a crystal mounted in a glass capillary using a copper rotating-anode X-ray generator (Mac Science) operated at 40 kV and 130 mA and equipped with an R-AXIS IV imaging-plate detector system (Rigaku) at 277 K. Exposures were performed for 2000 s per 2° oscillation for each diffraction frame using graphite-monochromated X-rays. Data sets were processed into intensities using the programs *DENZO* and *SCALEPACK* (Otwinowski & Minor, 1997). Data-collection statistics are summarized in Table 1.

2.3. Structure determination and refinement

The structure was determined by the molecular-replacement method using the program *X-PLOR* (Brünger, 1992). The 64M-2 Fab structure from the dT(6–4)T-liganded crystal (Yokoyama *et al.*, 2000) was used as a search model. Two solutions with the highest Patterson correlation value of 0.21 were obtained in the rotation search using an 8–4 Å resolution data set. This value was 2.6 times larger than that of the third solution. In the subsequent translation search, one of the solutions had a lower *R* factor (0.344) than the other (0.497) and placed the model in the proper location. The resultant model was subjected to rigid-body refinement with *X-PLOR* and the *R* value fell to 0.330. After a cycle of simulated annealing from 3000 to 300 K, *R* was 0.243 against 8–3 Å resolution data. In the course of *X-PLOR* refinement combined with model rebuilding with the program *TURBO-FRODO* (Roussel & Cambillau, 1995), reflections between 10 and 2.4 Å spacing were gradually added to the data set. After several cycles of refinement, individual *B* factors and ordered water molecules were included in the model.

Distinctive electron densities corresponding to the dTT(6–4)TT ligand were clearly discernible in the antigen-binding pocket. The structure of the T(6–4)T base moiety was derived from the crystal structure of 5-hydroxy-6–4′-(5′-methylpyrimid-2′-one)-dihydrothymine (Karle *et al.*, 1969) and was built into the model. The structural parameters for the deoxyribose, phosphate and normal thymine bases of dTT(6–4)TT were adopted from the standard DNA conformation (Parkinson *et al.*, 1996). In the vicinity of the light-chain N-terminal residue Asp1L, a clear peak with ten times the root-mean-square (r.m.s.) value of the $F_o - F_c$ electron density was ascribed to an Ni^{2+} ion derived from the crystallization solution.

The final model includes one Fab molecule with 432 residues, with the exception of a loop region consisting of Gly129H, Asp130H, Thr 133H and Thr134H in the constant region. The numbers of pairwise van der Waals contacts were calculated using the program *CONTACT* from the *CCP*4 suite (Winn *et al.*, 2011) with a cutoff distance of 4.0 Å. Solvent-accessible surface areas were calculated with *X-PLOR* (Brünger, 1992) using a probe radius of 1.6 Å. The atomic coordinates and structure-factor amplitudes have been deposited in the Protein Data Bank with the accession code 1keg.

3. Results and discussion

3.1. The structure of the 64M-2 Fab

The mean coordinate error in the structure determined at 2.4 Å resolution was estimated to be 0.32 Å from a σ_A plot (Read, 1986). Analysis of the main-chain torsion angles using *PROCHECK* (Laskowski *et al.*, 1993) placed 88% of residues in the favoured region of the Ramachandran plot. Only three residues, Val51L, Leu93L and Lys99H, were in the disallowed region. Val51L and Lys99H were also in the disallowed region in the dT(6–4)T-liganded 64M-2 Fab structure (Yokoyama *et al.*, 2000). Val51L is placed as a second residue in the γ-turn, which often exhibits unfavourable torsion angles (Milner-White *et al.*, 1988). Lys99H is placed in an environment packed by aromatic side chains. The conformation of Leu93L is attributable to a hydrogen bond to dTT(6–4)TT.

The Fab structure is virtually identical to the dT(6–4)T-liganded structure. The main-chain atoms of the variable region show a small r.m.s. positional difference of 0.52 Å between these structures. In the V_L–V_H interface, two pairs of hydrogen bonds are formed as observed in the dT(6–4)T-liganded structure: between the Glu34L and Arg95H side chains defined in clear electron densities, as shown in Fig. 2(*a*), and between the Gln38L and Gln39H side chains (Yokoyama *et al.*, 2000). The elbow angle relating the pseudo-dyads of the V_L/V_H variable and C_L/C_H1 constant regions is 176°, which is close to that of 174° in the dT(6–4)T-liganded structure. The variable region is hence in a nearly collinear arrangement with the constant region (Fig. 3). The complementarity-determining regions (CDRs) show the same canonical structure as the dT(6–4)T-liganded structure: the CDR loops L1, L2, L3, H1 and H2 are ascribable to canonical structures of types 4, 1, 3, 1 and 2, respectively (Chothia *et al.*, 1989).

3.2. Structure of dTT(6–4)TT

The dTT(6–4)TT molecule contains four consecutive thymidyl nucleotide residues, T1, T2, T3 and T4, arranged in the direction from the 5′-terminus to the 3′-terminus, with a (6–4) lesion at the central T2 and T3 residues. T1, T2 and T3 are defined by distinctive electron densities, as shown in Fig. 2(*b*), but the T4 residue is placed in low electron density. The T4 residue protrudes into the solvent region, possibly in multiple conformations. The central dT(6–4)T segment with a closed circular structure gives a small r.m.s. difference of 0.31 Å from that of the dT(6–4)T-liganded structure, indicating that the dT(6–4)T structure is not affected by the flanking nucleotides. The T2 base is in a half-chair conformation and the T3 base is in a nearly planar conformation. The six-membered ring planes of the T2 and T3 bases are nearly perpendicular to each other, with an interplanar angle of 77°. The torsion angles for the dTT(6–4)TT ligand are listed in Table 2. The glycosidic torsion angle χ of T3 is in a high-*anti* range, while those of T1, T2 and T4 are in an *anti* range (Saenger, 1984). The torsion angles γ of T2 and T3, which describe the direction of the O5′ atom relative to the C4′—C5′ bond (the atom numbering used is referred to Fig. 1), are both in a *gauche*$^+$ range and those of T1 and T4 are in an *anti* range.

Table 2
Torsion angles for the dTT(6–4)TT ligand.

Segment	Definition	Angle (°)† T1	T2	T3	T4
Glycosidic linkage	χ (O4′—C1′—N1—C2)	−156	−109 (−138/−118)	−60 (−75/−86)	123
Sugar-phosphate backbone	α (O3′—P—O5′—C5′)	—	−47	−99 (−96/−78)	−70
	β (P—O5′—C5′—C4′)	—	−168	−141 (−177/174)	−173
	γ (O5′—C5′—C4′—C3′)	168	40 (56/−159)	38 (43/46)	163
	δ (C5′—C4′—C3′—O3′)	147	110 (80/77)	126 (100/94)	153
	ε (C4′—C3′—O3′—P)	−138	−150 (−107/−130)	−151	—
	ζ (C3′—O3′—P—O5′)	−75	−71 (−76/−73)	78	—
(6–4) linkage‡	N1—C6—C4#—C5#	−139 (—/−122)			
	N1—C6—C4#—N3#	38 (27/35)			
	(C5 methyl)—C5—C6—C4#	−152 (−163/−159)			

† T1, T2, T3 and T4 represent the four thymidines of dTT(6–4)TT, designated in the direction from the 5′-terminus to the 3′-terminus. The first values in parentheses are for the isolated dT(6–4)T in solution (Taylor *et al.*, 1988; Kim *et al.*, 1995). The second values in parentheses are for the T(6–4)T segment in the (6–4) photolyase–DNA complex (Maul *et al.*, 2008; PDB entry 3cvu). ‡ Atoms of T3 are marked #.

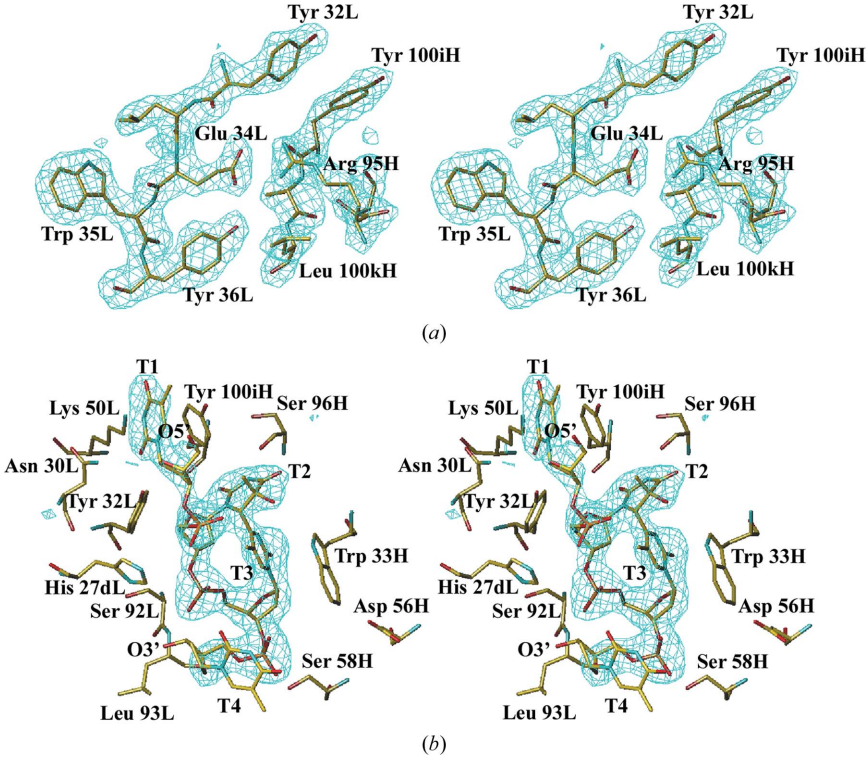

Figure 2
Stereo drawings of $F_o - F_c$ electron-density maps. Each of the maps is calculated based on phases from the model without the residues shown here and is contoured at the 3σ level. (*a*) The V_L–V_H interface around Glu34L. The map is superposed on a stick model for residues 32L–36L, 95H–96H and 100iH–100kH. (*b*) Electron density of dTT(6–4)TT. T1, T2, T3 and T4 represent the four consecutive thymidines from the 5′-terminus to the 3′-terminus. O5′ and O3′ represent the 5′-terminal and 3′-terminal O atoms, respectively. The Fab residues in the vicinity of the ligand are also shown as stick models. Figs. 2–4 were produced using the program *TURBO-FRODO* (Roussel & Cambillau, 1995).

These angles reflect the ligand structure, in which the dT(6–4)T segment is compactly lobed and the adjacent T1 and T4 are expelled from the segment. Three pairs of the ζ and α torsion angles for the phosphodiester bonds are in a *gauche*$^-$ range, with the exception being the ζ angle of T3, which is in a *gauche*$^+$ range. If the ζ angle of T3 is in a *gauche*$^-$ range, the T4 deoxyribose would be directed towards a location that causes steric hindrance with the Asp56H side chain (Fig. 2*b*).

As for the deoxyribose puckers, the T2 deoxyribose is in a C3′-*endo* conformation and the T3 deoxyribose is in a nearly planar conformation, as observed for the dT(6–4)T ligand. Both the T1 and T4 deoxyriboses are in a C2′-*endo* conformation, which corresponds to the regular B-form of DNA.

As shown in Table 2, the conformation of the dT(6–4)T segment is almost the same as those of isolated dT(6–4)T in the solution structure (Taylor *et al.*, 1988; Kim *et al.*, 1995) and the dT(6–4)T segment in the (6–4) photolyase–DNA complex (Maul *et al.*, 2008). The torsion angle γ of T2 in the (6–4) photolyase–DNA complex is different from the other two structures because the dT(6–4)T segment is flipped out of the duplex.

3.3. Interaction between dTT(6–4)TT and Fab

A total of 16 residues from the six CDR loops are involved in binding to the ligand (Fig. 4). The T2 base is perpendicular to the Tyr100iH side chain, accounting for 11 van der Waals contacts. The O2 atom of the T2 base is hydrogen bonded to the Arg95H N$^{\varepsilon}$ atom and the N3 atom is hydrogen bonded to Ser96H O. The O4 atom is hydrogen bonded to Wat61, which is hydrogen bonded to the Trp33H N and Arg95H O atoms. The T3 base makes a stacking interaction with the indole ring of Trp33H with a face-to-face interplanar distance of 3.5 Å, accounting for 16 contacts. The O2 atom of the T3 base is hydrogen bonded to His35H N$^{\varepsilon 2}$ and is also in contact with Wat59, which is hydrogen bonded to Gly91L O. The O1P atom of the phosphate group connecting T2 and T3 is hydrogen bonded to Leu93L N. The T2 deoxyribose is in close proximity to the Tyr32L side chain, accounting for 13 contacts. Two water molecules, 59 and 61, are also located in the corresponding locations in the dT(6–4)T-liganded structure.

In the (6–4) photolyase–DNA complex (Maul *et al.*, 2008), the 5′-thymine (corresponding to T2) base is hydrogen bonded to the side chains of Gln299 and His365, while no hydrogen bonds are observed in the 3′-pyrimidone (corresponding to

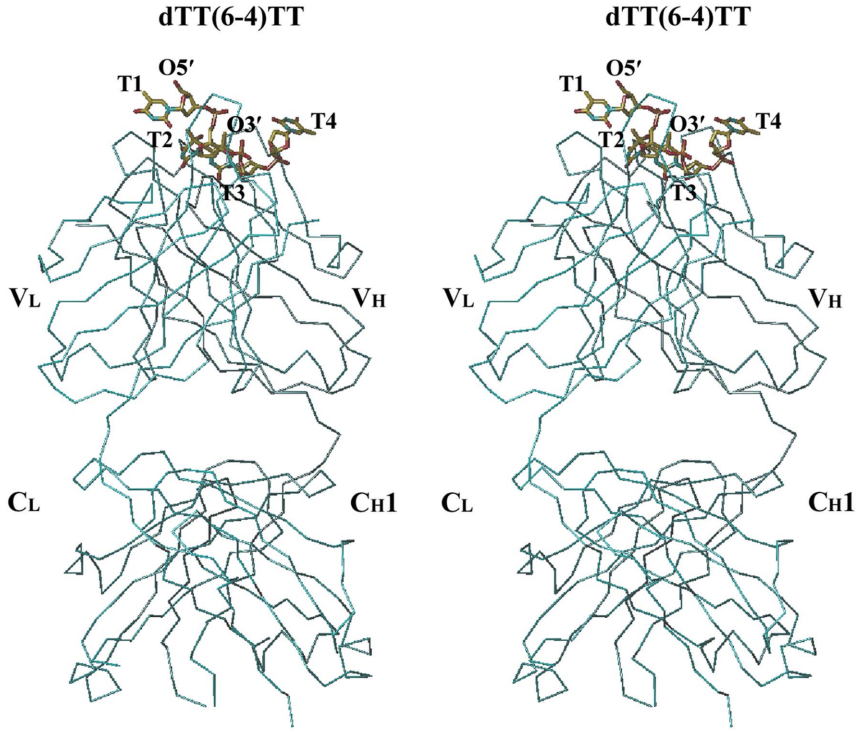

Figure 3
Stereo C^{α} trace of the 64M-2 Fab structure. The bound dTT(6–4)TT is represented as a stick model. The Fab domains are labelled V_L, V_H, C_L and C_H1.

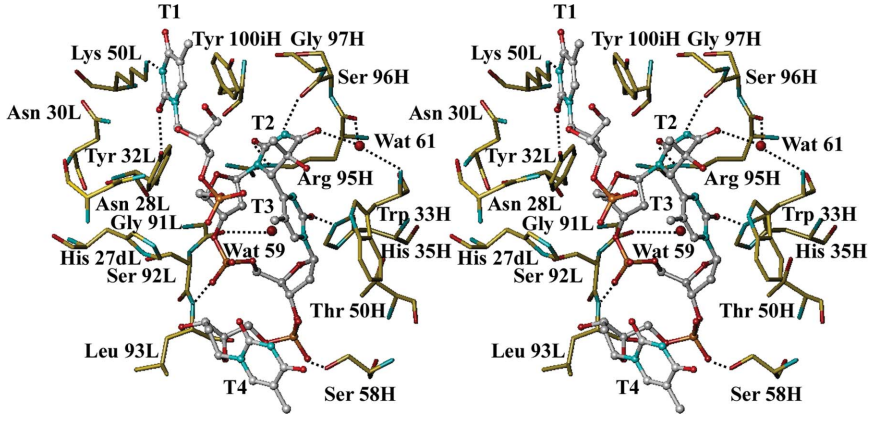

Figure 4
Stereo drawing of the antigen-binding site of the 64M-2 Fab in complex with dTT(6–4)TT. The Fab residues are represented as sticks, ligand residues as ball-and-stick representations with C atoms in grey and water molecules as red spheres. Hydrogen bonds are shown as broken lines.

T3) base. The hydrophobic residues Trp302, Trp409, Pro247, Pro293 and Val294 form a side wall of the pocket and interact with the 5′-thymime and 3′-pyrimidone bases. The Arg421 side chain protrudes into the duplex and interacts with the phosphate of the dT(6–4)T segment. A major similarity between the 64M-2 antibody and (6–4) photolyase structures is that the 5′-thymine base is recognized by hydrogen-bonding and aromatic–aromatic interactions, although the interacting residues are not conserved between the antibody and the photolyase. The O2 and N3 atoms of the T2 base are hydrogen bonded to Arg side-chain and main-chain atoms in the 64M-2 antibody as described above, while the O2, N3 and C5 OH atoms are hydrogen bonded to Gln and His side chains in the photolyase structure (Maul *et al.*, 2008). On the other hand, differences are observed in the orientation of the dT(6–4)T segment. In the 64M-2 Fab–dTT(6–4)TT structure, the whole dT(6–4)T segment, including bases, phosphate and sugars, is accommodated in the binding pocket, as shown in Fig. 4. In the (6–4) photolyase the base moiety of the dT(6–4)T segment is plunged into the pocket, while the sugar-phosphate moiety is left at the surface of the pocket. This is because the dT(6–4)T segment is flipped out of the duplex DNA in the photolyase structure.

The terminal T1 and T4 thymidines show relatively large average *B* factors (45 and 51 Å^2, respectively), in marked contrast to T2 (25 Å^2) and T3 (20 Å^2). The T2 and T3 residues are accommodated in the concave binding pocket of the Fab. The high *B* factors for T1 and T4 are a consequence of their protrusion from the pocket (Fig. 3). Out of the 147 contacts between the ligand, Fab and water molecules, the T4 thymidine accounts for only 12 contacts and its base is not involved in the contacts. The O2P atom of the phosphate group between T3 and T4 is hydrogen bonded to Ser58H O^{γ}. The O2 atom of the T1 base is hydrogen bonded to Tyr32L O^{η}. The O2 atom also interacts with Asn30L $N^{\delta2}$. Lys50L N^{ζ} exhibits electrostatic interactions with the O2, N3 and O4 atoms of the T1 base, with distances of 3.2, 2.6 and 3.6 Å, respectively. The short distance for the N3 atom suggests the formation of a hydrogen bond between Lys50L N^{ζ} and the imino N3 of an enol form of the T1 base. The T1 base is nearly parallel to the Tyr100iH side chain, accounting for 14 contacts. The O3′ atom of the T1 deoxyribose interacts with Asn28L $N^{\delta2}$. The $N^{\varepsilon2}$ atom of the basic side chain of His27dL shows an electrostatic interaction with the phosphate O atom O1P with a distance of 3.6 Å.

The antibody residues involved in interactions with the ligand are mostly conserved in the homologous 64M-5 antibody, which shows high sequence identity to the variable regions of 64M-2: 96% for V_L and 88% for V_H (Morioka *et al.*, 1998). Among the residues involved in binding the ligand, those in 64M-5 that differ from 64M-2 are Tyr30L, Thr50L, His93L, Thr58H, Asn96H and Tyr97H. In the 64M-2 Fab the main-chain atoms of Leu93L and Ser96H are involved in the binding. The Ser58H side chain of 64M-2 is hydrogen bonded to the ligand and thus the Thr58H side chain of 64M-5 is also

presumed to be hydrogen bonded to the ligand. Hence, these antibodies are judged to have a common structural construction for ligand binding.

3.4. Comparison with the nucleotide-binding antibody Jel103

The crystal structure of the Fab of the anti-RNA antibody Jel103 has been reported in complex with the rGDP ligand (Pokkuluri *et al.*, 1994). The 64M-2 antibody shows high sequence identity to the variable regions of Jel103: 92% for V_L and 73% for V_H. When the variable domains of Jel103 are superimposed on those of the 64M-2 Fab, the rGDP ligand is placed near the T1 residue of dTT(6–4)TT. The rGDP and T1 structures interact mainly with residues in nearly identical sequences and locations as those of their cognate antibodies: Asn28L, Tyr32L and Lys50L are identical and Ser91L of Jel103 is in nearly the same location as Gly91L of 64M-2. However, the nucleotide ligands are orientated in different directions relative to the binding pockets. The T1 base is pointing away from the pocket, but the guanine base of rGDP plunges into the pocket. The rGDP guanine base interacts with Tyr32L and Ser91L of the Jel103 Fab and the sugar-phosphate backbone interacts with Asn28L and Lys50L. This binding contrasts with the dTT(6–4)TT complex; the T1 base interacts with Tyr32L and Lys50L and the sugar-phosphate backbone interacts with Asn28L and Tyr32L (Fig. 4). The Arg96H side chain of Jel103 is situated so as to cover the rGDP sugar-phosphate backbone. In the 64M-2 structure the Tyr100iH side chain is situated nearly parallel to the T1 base. These V_H residues possibly play significant roles in specific recognition of the antigen ligands.

3.5. Increased affinity of dTT(6–4)TT

A higher affinity of the 64M-5 Fab has been reported for longer oligonucleotides of up to a hexamer containing the dT(6–4)T segment in the centre (Kobayashi *et al.*, 1998). For the dAT(6–4)TA ligand, the binding affinity has been reported to be $3.1 \times 10^8\ M^{-1}$, which is about 70 times higher than for the dT(6–4)T ligand. In the dT(6–4)T complex with the 64M-2 Fab, five CDR loops (the exception being L2) are involved in binding. In the dTT(6–4)TT complex all six CDR loops are involved; Lys50L of L2 participates in the electrostatic interaction with the T1 base that is parallel to the Tyr100iH side chain. The dTT(6–4)TT ligand makes a total of 147 contacts, far outnumbering the 103 contacts of the dT(6–4)T ligand.

The T4 base has a large average *B* factor (62 Å^2), while that of its sugar-phosphate backbone is 40 Å^2. The T1 base and backbone atoms have average *B* factors of 44 and 46 Å^2, respectively. The flanking T1 and T4 thymidines, which have large *B* factors in the liganded structure, possibly interact with these Fabs in a less base-specific manner, but their adjoining phosphate groups are involved in electrostatic interactions with the Fab residues. These interactions retained by the flanking nucleotides, mostly by the T1 base and the phosphate groups on both sides of the dT(6–4)T segment, constitute an enthalpic contribution to the increased binding affinity. The surface area of Fab interfaced with the dTT(6–4)TT ligand is 450 Å^2, which is much greater than that in the dT(6–4)T complex (258 Å^2). The increased affinity is also ascribable to the increase in surface area, which contributes to an entropic stabilization of free energy upon complexation with the antibodies.

Elucidation of the structure of the DNA photoproduct dTT(6–4)TT in complex with the antibody Fab shows that the central dT(6–4)T segment is fully accommodated in the concave pocket. This structure of the binding pocket is responsible for the specific recognition of the (6–4) lesion. The flanking 5′-side thymidylate and 3′-side phosphate groups are responsible for the increased affinity of the dTT(6–4)TT ligand. These interactions involving the flanking nucleotides as well as specific recognition of the central (6–4) lesion explain why longer oligonucleotides containing dT(6–4)T segments in the centre show higher antibody-binding affinities than the dT(6–4)T ligand.

This work was supported by a Grant-in-Aid for Specially Promoted Research (No. 08101001) to YS and also by a Grant-in-Aid for Young Scientists (B) (No. 21770122) to HY from the Ministry of Education, Culture, Sports, Science and Technology, Japan.

References

Brünger, A. T. (1992). *X-PLOR Version 3.1: A System for X-ray Crystallography and NMR*. New Haven: Yale University Press.
Chothia, C., Lesk, A. M., Tramontano, A., Levitt, M., Smith-Gill, S. J., Air, G., Sheriff, S., Padlan, E. A., Davies, D., Tulip, W. R., Colman, P. R., Spinelli, S., Alzari, P. M. & Poljak, R. J. (1989). *Nature (London)*, **342**, 877–883.
Iwai, S., Shimizu, M., Kamiya, H. & Ohtsuka, E. (1996). *J. Am. Chem. Soc.* **118**, 7642–7643.
Kabat, E. A., Wu, T. T., Perry, H. M., Gottesman, K. S. & Foeller, C. (1991). *Sequences of Proteins of Immunological Interest*, 5th ed. Bethesda: National Institutes of Health.
Karle, I. L., Wang, S. Y. & Varghese, A. J. (1969). *Science*, **164**, 183–184.
Kim, J.-K., Patel, D. & Choi, B.-S. (1995). *Photochem. Photobiol.* **62**, 44–50.
Kobayashi, H., Morioka, H., Tobisawa, K., Torizawa, T., Kato, K., Shimada, I., Nikaido, O., Stewart, J. D. & Ohtsuka, E. (1999). *Biochemistry*, **38**, 532–539.
Kobayashi, H., Morioka, H., Torizawa, T., Kato, K., Shimada, I., Nikaido, O. & Ohtsuka, E. (1998). *J. Biochem.* **123**, 182–188.
Laskowski, R. A., MacArthur, M. W., Moss, D. S. & Thornton, J. M. (1993). *J. Appl. Cryst.* **26**, 283–291.
LeClerc, J. E., Borden, A. & Lawrence, C. W. (1991). *Proc. Natl Acad. Sci. USA*, **88**, 9685–9689.
Lee, J.-H., Hwang, G.-S. & Choi, B.-S. (1999). *Proc. Natl Acad. Sci. USA*, **96**, 6632–6636.
Maul, M. J., Barends, T. R. M., Glas, A. F., Cryle, M. J., Domratcheva, T., Schneider, S., Schlichting, I. & Carell, T. (2008). *Angew. Chem. Int. Ed.* **47**, 10076–10080.
Milner-White, E., Ross, B. M., Ismail, R., Belhadj-Mostefa, K. & Poet, R. (1988). *J. Mol. Biol.* **204**, 777–782.
Mori, T., Nakane, M., Hattori, T., Matsunaga, T., Ihara, M. & Nikaido, O. (1991). *Photochem. Photobiol.* **54**, 225–232.
Morioka, H., Miura, H., Kobayashi, H., Koizumi, T., Fujii, K., Asano, K., Matsunaga, T., Nikaido, O., Stewart, J. D. & Ohtsuka, E. (1998). *Biochim. Biophys. Acta*, **1385**, 17–32.
Otwinowski, Z. & Minor, W. (1997). *Methods Enzymol.* **276**, 307–326.

Parkinson, G., Vojtechovsky, J., Clowney, L., Brünger, A. T. & Berman, H. M. (1996). *Acta Cryst.* D**52**, 57–64.
Pokkuluri, P. R., Bouthillier, F., Li, Y., Kuderova, A., Lee, J. & Cygler, M. (1994). *J. Mol. Biol.* **243**, 283–297.
Read, R. J. (1986). *Acta Cryst.* A**42**, 140–149.
Roussel, A. & Cambillau, C. (1995). *TURBO-FRODO* v.5.4. Faculté de Médecine Nord, Marseille, France.
Rycyna, R. E. & Alderfer, J. L. (1985). *Nucleic Acids Res.* **13**, 5949–5963.
Saenger, W. (1984). *Principles of Nucleic Acid Structure*, pp. 14–24. New York: Springer-Verlag.
Scrima, A., Konícková, R., Czyzewski, B. K., Kawasaki, Y., Jeffrey, P. D., Groisman, R., Nakatani, Y., Iwai, S., Pavletich, N. P. & Thomä, N. H. (2008). *Cell*, **135**, 1213–1223.
Setlow, R. B. (1978). *Nature (London)*, **271**, 713–717.
Taylor, J.-S., Garrett, D. S. & Wang, M. J. (1988). *Biopolymers*, **27**, 1571–1593.
Torizawa, T., Kato, K., Kimura, Y., Asada, T., Kobayashi, H., Komatsu, Y., Morioka, H., Nikaido, O., Ohtsuka, E. & Shimada, I. (1998). *FEBS Lett.* **429**, 157–161.
Weber, S. (2005). *Biochim. Biophys. Acta*, **1707**, 1–23.
Winn, M. D. *et al.* (2011). *Acta Cryst.* D**67**, 235–242.
Yokoyama, H., Mizutani, R., Satow, Y., Komatsu, Y., Ohtsuka, E. & Nikaido, O. (2000). *J. Mol. Biol.* **299**, 711–723.